Method to find the electron distribution function from cylindrical probe data

Scott Knappmiller and Scott Robertson
Department of Physics, University of Colorado, Boulder, Colorado 80309-0390, USA

Zoltan Sternovsky
Laboratory for Atmospheric and Space Physics, University of Colorado, Boulder, Colorado 80309-0392, USA

(Received 6 February 2006; published 7 June 2006)

Druyvesteyn's method finds the distribution of electron speeds from the second derivative of probe data using the assumption that the distribution is spherically symmetric. For the disk probe, the data are more directly related to the velocity distribution projected onto the direction normal to the probe surface. The projected distribution is less sensitive to noise because it is related to the first derivative of the data rather than the second. For the cylindrical probe, the data are more directly related to the distribution of energies projected onto the plane perpendicular to the probe axis. A method is developed for recovering this projected distribution from digitized probe data. The method is mathematically more complex than Druyvesteyn's method, but has the advantage of being less sensitive to noise. The methods are compared using noise-free simulated data and using noisy data from a double-plasma device with multidipolar magnetic confinement.

DOI: 10.1103/PhysRevE.73.066402 PACS number(s): 52.70.Ds

I. INTRODUCTION

In 1930, Druyvesteyn [1] published relationships that allowed the distribution of electron speeds to be found from Langmuir probe characteristics. The distribution that is found is often integrated to find the plasma density. Druyvesteyn's method is especially valuable for non-Maxwellian plasmas [2,3] for which the density is not simply related to an electron temperature and the probe saturation current. A disadvantage of the method is that it uses the second derivative of the probe data, which is strongly affected by noise. Useful results are usually obtained only after averaging many probe data sets or after smoothing the data mathematically. The disk probe acts as a retarding potential analyzer and the data are simply related to the distribution of electron velocities projected onto the normal to the probe surface. This projected distribution is easily recovered from the first derivative of the probe data, which is less sensitive to noise. The projected distribution may be integrated to obtain the plasma density. In this work, a relationship is derived between the data from a cylindrical probe and the distribution of velocities projected onto the plane perpendicular to the probe axis. The inverse relation is also derived, which allows the projected distribution to be found from the probe data. The method is mathematically more complex than Druyvesteyn's method, but is less sensitive to noise and is easily implemented in a mathematical spreadsheet.

In Sec. II A, the relationships between the distribution functions and the probe data are reviewed for the disk probe. Finite-difference methods are derived for recovering the velocity distribution when it is spherically symmetric, and for recovering the distribution projected onto the axis normal to the probe surface. In Sec. II B, a new relationship is derived between data from a cylindrical probe and the distribution of velocities projected onto the plane perpendicular to the probe axis. Finite-difference methods are derived that allow the projected distribution to be recovered from probe data. For comparison, Druyvesteyn's method is derived using the same notation. In Sec. III, numerical methods are used to construct simulated probe data that would be obtained by disk and cylindrical probes in plasma with a two-temperature distribution. The two disk and two cylindrical probe methods are shown to correctly recover the distribution functions and the plasma density. In Sec. IV, the methods are applied to experimental data from a double-plasma device that has a two-temperature electron distribution and the sensitivities of the methods to noise are compared. Section V is a discussion and conclusion.

II. RELATIONSHIPS BETWEEN THE PROBE CURRENT AND DISTRIBUTION FUNCTIONS

In this section, we derive the relationships between probe characteristics and distribution functions for disk and cylindrical probes biased with negative potentials Φ that retard electrons. The potential Φ is measured relative to the plasma potential. The spherical probe is not discussed because it is rarely used in experiments.

A. Disk probe

Electrons approaching a sufficiently large planar disk probe oriented perpendicular to the z axis have only their z component of velocity changed by the probe bias potential. It is appropriate to use a one-dimensional distribution function $f_1(v_z)$ in which two velocity components have been removed by integration. The number density of electrons with velocity between v_z and v_z+dv_z is

$$dn = f_1(v_z)dv_z, \tag{1}$$

and the contribution of these electrons to the probe current is

$$dI = qv_zAdn, \tag{2}$$

where q is the absolute value of the charge, A is the probe area, and the subscript 1 denotes a one-dimensional velocity space. The current to the probe is found by integration over

v_z, omitting the electrons with insufficient energy to strike the probe surface

$$I(\Phi) = Aq \int_{u(\Phi)}^{\infty} f_1(v_z) v_z dv_z, \tag{3}$$

where $u(\Phi) = \sqrt{-2q\Phi/m}$ is the minimum electron velocity that will be collected and m is the electron mass. A change of variables gives

$$I(\Phi) = \frac{Aq}{m} \int_{-q\Phi}^{\infty} f_1(\epsilon) d\epsilon, \tag{4}$$

where $\epsilon = \frac{1}{2} m v_z^2$ is the electron kinetic energy in the z direction, and $f_1(\epsilon)$ is $f_1(v_z)$ written as a function of energy [to avoid the cumbersome $f_1(\sqrt{2\epsilon/m})$]. The velocities of electrons decrease as they approach the negatively biased probe and their density dn increases. Continuity in one dimension requires that the current remain constant. Thus the current may be calculated from the velocities v_z and densities dn evaluated at infinity rather than at the probe surface.

The derivative of the current with respect to bias potential is

$$f_1(-q\Phi) = \frac{m}{q^2 A} \frac{dI(\Phi)}{d\Phi}. \tag{5}$$

It is assumed that the ion contribution to $I(\Phi)$ has been removed. For probe data that have been digitized, derivatives are most easily obtained using finite differences. The projected distribution f_1 is

$$f_1(-q\Phi_{k-1/2}) = \frac{m}{q^2 A} \left(\frac{I_k - I_{k-1}}{\Phi_k - \Phi_{k-1}} \right), \tag{6}$$

where, for second-order accuracy, the potential at the midpoint of the interval $\Phi_{k-1/2} = 0.5(\Phi_k + \Phi_{k-1})$ has been used. The electron density is found by integrating the distribution function by the midpoint method to obtain

$$n = 2 \int_0^{\infty} f_1(\epsilon) \frac{d\epsilon}{\sqrt{2m\epsilon}} = \frac{2m}{qA} \int \frac{(dI/d\Phi)}{\sqrt{-2mq\Phi}} d\Phi, \tag{7}$$

where $\Delta\Phi = \Phi_k - \Phi_{k-1}$. The final expression is implemented for discrete data in a mathematical spreadsheet in which cubic splines are fit to $I(\Phi)$ to obtain a continuous function and differentiated to obtain $dI/d\Phi$. The spreadsheet is also used for the integration from the most negative probe voltage to the plasma potential. Integration by Simpson's rule was found to give densities 10–20 % lower, possibly because of the divergent behavior of the inverse square root function.

Druyvesteyn used the distribution of speeds $\rho(v)$ with normalization [4]

$$n = \int_0^{\infty} \rho(v) dv, \tag{8}$$

where a factor of $4\pi v^2$ is contained within $\rho(v)$. He found the flux of electrons to the probe surface using Boltzmann's method for finding the momentum flux [5] to a surface with the addition of cutoffs to the ranges of integration. The normal component of velocity is written as $v \cos\alpha$, where α is the polar angle measured from the normal to the surface. The collected current is

$$I(\Phi) = Aq \int_u^{\infty} \rho(v) \int_0^{\theta(v)} \frac{1}{2} v \cos\alpha \sin\alpha d\alpha dv, \tag{9}$$

where v without a subscript is the speed and the ranges of integration are coupled by the relation $-q\Phi < \frac{1}{2} m v^2 \cos^2\theta$. Integration over angle α gives

$$I(\Phi) = \frac{Aq}{4} \int_u^{\infty} \rho(v) \left(1 + \frac{2q\Phi}{mv^2} \right) v dv. \tag{10}$$

The inverse relation is obtained from two differentiations,

$$\rho(-q\Phi) = -\frac{4m\Phi}{q^2 A} \frac{d^2 I(\Phi)}{d\Phi^2}, \tag{11}$$

where $\rho(-q\Phi)$ is $\rho(v)$ written as a function of energy. In finite-difference form, Eq. (11) becomes

$$\rho(-q\Phi_k) = -\frac{4m\Phi}{q^2 A} \left[\frac{I(\Phi_{k+1}) - 2I(\Phi_k) + I(\Phi_{k-1})}{(\Delta\Phi)^2} \right], \tag{12}$$

and the density is found from $\rho(-q\Phi)$ using Simpson's method

$$n = \sum_k \frac{1}{2} \left\{ \frac{\rho(-q\Phi_k)}{\sqrt{2mq\Phi_k}} + \frac{\rho(-q\Phi_{k-1})}{\sqrt{2mq\Phi_{k-1}}} \right\} (q\Phi_k - q\Phi_{k-1}), \tag{13}$$

where the sum goes from the most negative voltage to zero voltage. The final term in the sum that is for zero probe voltage is not evaluated, but is set to zero using L'Hopital's rule. The expression for the second derivative in Eq. (12) is correct only for uniformly spaced data points.

B. Cylindrical probe

Electrons approaching a negatively biased cylindrical probe are deflected and collection depends upon both the energy and angular momentum. The velocity v_z parallel to the probe axis does not affect collection and can be removed by integration. The number density of electrons with velocity between v_r and $v_r + dv_r$ is

$$dn = 2\pi f_2(v_r) v_r dv_r, \tag{14}$$

where v_r is the velocity in the plane perpendicular to the probe axis and the subscript 2 denotes cylindrical symmetry. For a monoenergetic distribution and a negative probe bias, orbit-motion-limited (OML) theory of Mott-Smith and Langmuir [6] shows that the current density at the probe surface is reduced because the electron trajectories are deflected away from the probe axis. The current collected from a monoenergetic beam of electrons with sufficient energy is [7]

$$dI = 2aLqv_r \left(1 + \frac{q\Phi}{\frac{1}{2} m v_r^2} \right)^{1/2} dn, \quad \frac{1}{2} m v_r^2 \geq -q\Phi, \tag{15}$$

where a is the probe radius, L is the probe length, and $2aL$ is the area of the probe in projection seen by the beam. The net current from a distribution of electrons is

$$I(\Phi) = 4\pi aLq\int_u^\infty f_2(v_r)\left(1+\frac{2q\Phi}{mv_r^2}\right)^{1/2} v_r^2 dv_r$$
$$= \frac{2Aq}{m}\left(\frac{2}{m}\right)^{1/2}\int_{-q\Phi}^\infty f_2(\epsilon)(q\Phi+\epsilon)^{1/2}d\epsilon, \qquad (16)$$

where $A=2\pi aL$ is the probe surface area. The first derivative of the current is

$$\frac{dI(\Phi)}{d\Phi} = \frac{Aq^2}{m}\left(\frac{2}{m}\right)^{1/2}\int_{-q\Phi}^\infty \frac{f_2(\epsilon)d\epsilon}{\sqrt{q\Phi+\epsilon}}, \qquad (17)$$

which contains an integrable singularity. There is not a simple relationship between the distribution function f_2 and the derivative of the probe data as there is in the planar case.

Finite-difference methods are used to find the relationship between $I(\Phi)$ and $f_2(\epsilon)$. The integral for $I(\Phi)$ in Eq. (16) is first broken into a sum of integrals performed over the small intervals in energy determined by the digitized probe voltages

$$I(\Phi_k) = \frac{2Aq}{m}\left(\frac{2}{m}\right)^{1/2}\sum_{j=1}^k \int_{-q\Phi_j}^{-q\Phi_{j-1}} f_2(\epsilon)[q\Phi_k+\epsilon]^{1/2}d\epsilon. \qquad (18)$$

The zeroth probe potential Φ_0 is assumed to be the most negative. The electron energy $-q\Phi_0$ corresponding to the most negative probe voltage replaces the infinity that is one limit of the integral.

Finite-difference methods are accurate only when the contributions of the omitted higher-order derivatives are negligible. The square root function, however, has the property that the higher-order derivatives diverge for arguments near zero. Thus numerical integration yields results that are significantly in error for $q\Phi+\epsilon$ near zero. The function $f_2(\epsilon)$, which is assumed to vary smoothly, is taken through the integral sign using the value at the midpoint of the interval. The remaining square root function is integrated analytically to obtain

$$I(\Phi_k) = \frac{2Aq}{m}\left(\frac{2}{m}\right)^{1/2}\sum_{j=1}^k f_2(-q\Phi_{j-1/2})\int_{-q\Phi_j}^{-q\Phi_{j-1}}[q\Phi_k+\epsilon]^{1/2}d\epsilon$$
$$= \frac{2Aq}{m}\left(\frac{2}{m}\right)^{1/2}\sum_{j=1}^k f_2(-q\Phi_{j-1/2})\left\{\frac{2}{3}[q\Phi_k-q\Phi_{j-1}]^{3/2} - \frac{2}{3}[q\Phi_k-q\Phi_j]^{3/2}\right\}, \qquad (19)$$

which contains no singularities. The solution of Eq. (19) for $f_2(-q\Phi_{k-1/2})$ is

$$f_2(-q\Phi_{k-1/2}) = \frac{\left(\frac{I(\Phi_k)m}{2Aq}\right)\left(\frac{m}{2}\right)^{1/2} - \sum_{j=1}^{k-1} f_2(-q\Phi_{j-1/2})\left\{\frac{2}{3}[q\Phi_k-q\Phi_j]^{3/2} - \frac{2}{3}[q\Phi_k-q\Phi_{j-1}]^{3/2}\right\}}{\frac{2}{3}[q\Phi_k-q\Phi_{k-1}]^{3/2}}. \qquad (20)$$

The solution at each k value requires the kth probe current and the values for the distribution function found at the smaller values of k. The first two values of f_2 are defined as $f_2(-q\Phi_{1/2})=0$ and as

$$f_2(-q\Phi_{3/2}) = \frac{\left(\frac{I(\Phi_1)m}{2Aq}\right)\left(\frac{m}{2}\right)^{1/2}}{\frac{2}{3}[q\Phi_1-q\Phi_0]^{3/2}}. \qquad (21)$$

The subsequent values of the distribution function are built up sequentially using Eq. (20).

The complicated relationship in Eq. (20) arises in the following way. If the probe voltage is increased from Φ_k to Φ_{k+1}, the current increases (i) because of new electrons collected with energy between $-q\Phi_k$ and $-q\Phi_{k+1}$, and (ii) because of additional current from the increased collection of the more energetic electrons. In the numerator of Eq. (20), the contribution to the current from the more energetic electrons is calculated from the distribution function and is subtracted from the measured current at Φ_k to obtain the part of the current that is from electrons with energy between Φ_k and Φ_{k+1}.

The electron density is obtained from $f_2(\epsilon)$ by numerical integration using the midpoint method

$$n = 2\pi\int_0^\infty f_2(\epsilon)\frac{d\epsilon}{m} = \frac{2\pi}{m}\sum_{j=1}^k (-q\Phi_j+q\Phi_{j-1})f_2(-q\Phi_{j-1/2}). \qquad (22)$$

Druyvesteyn found the relation between the probe data and the distribution of speeds $\rho(v)$ without finding the expression for the probe current. Mott-Smith and Langmuir [6] showed that the current density at the probe surface is different from the current density $qv\,dn$ at infinity by the factor $(1+2q\Phi/mv^2)$ in the spherical case and $(1+2q\Phi/mv^2)^{1/2}$ in the cylindrical case. The current to the cylindrical probe expressed as a function of $\rho(v)$ is

$$I(\Phi) = \frac{Aq}{\pi}\int_u^\infty \rho(v)\int_{\theta(v)}^{\pi-\theta(v)}\left(1+\frac{2q\Phi}{mv^2\sin^2\alpha}\right)^{1/2} \times\frac{1}{2}v\sin^2\alpha d\alpha dv$$
$$= \frac{Aq}{\pi}\int_u^\infty \rho(v)\int_{\theta(v)}^{\pi/2}[(1-u^2/v^2)-\cos^2\alpha]^{1/2}v\sin\alpha d\alpha dv$$
$$= \frac{Aq}{4}\int_u^\infty \rho(v)\left(1+\frac{2q\Phi}{mv^2}\right)v dv, \quad (23)$$

where the velocity in the plane perpendicular to the probe axis is $v_r = v\sin\alpha$ and α is the polar angle measured from the probe axis. The minimum electron velocity is $u=\sqrt{-2q\Phi/m}$ and for velocities $v>u$ the permitted angles of incidence have $\sin\theta(v)\geq u/v$. The first derivative of the probe current is

$$\frac{dI}{d\Phi} = \frac{q^2A}{4m}\int_{-q\Phi}^\infty \rho(\epsilon)\frac{d\epsilon}{\epsilon}, \quad (24)$$

and from the second derivative the speed distribution is

$$\rho(\epsilon) = \frac{-4m\Phi}{q^2A}\frac{d^2I}{d\Phi^2} = \frac{-4m\Phi}{q^2A}\left[\frac{I(\Phi_{k+1})-2I(\Phi_k)+I(\Phi_{k-1})}{(\Delta\Phi)^2}\right], \quad (25)$$

which is the result obtained by Druyvesteyn expressed both in standard form and finite-difference form. From this distribution, n is found using Eq. (13).

III. ANALYSIS OF SIMULATED DATA SETS

The four methods of finding a distribution function, Eqs. (6), (11), (20), and (25), and three methods for finding the density, Eqs. (7), (13), and (22), are tested in this section using simulated data sets. The simulated sets have the advantage of being free of noise that might obscure details in the distribution functions. In many laboratory plasmas, the electrons are confined by a positive plasma potential Φ_p. Electrons with energy below $q\Phi_p$ may be confined for many self-collision times and the distribution function for these electrons will become nearly Maxwellian. Electrons with energy above $q\Phi_p$ will have a shorter confinement time and will not have equilibrated, thus their energy distribution will be determined by the mechanism that created them, such as secondary emission from the chamber surfaces [11]. The slope of the combined distributions is likely to be discontinuous at the energy $-q\Phi_p$. For these reasons, the methods of analysis are tested using a two-temperature distribution

$$f_3(v) = n\left(\frac{m}{2\pi T_1}\right)^{3/2}\exp\left(\frac{-mv^2}{2T_1}\right), \quad \frac{1}{2}mv^2 < \epsilon_t$$
$$= n\left(\frac{m}{2\pi T_2}\right)^{3/2}\exp\left(\frac{-mv^2}{2T_2}+\frac{\epsilon_t}{T_2}-\frac{\epsilon_t}{T_1}\right), \quad \frac{1}{2}mv^2 \geq \epsilon_t \quad (26)$$

with $n=10^{14}$ m^{-3}, $T_1=0.2$ eV, and $T_2=2$ eV. The parameter $\epsilon_t=2$ eV is the energy at which the slope of the distribution changes. The number density is negligibly larger than n as a consequence of the small number of particles in the high-temperature tail. The corresponding speed distribution is $\rho(v)=4\pi v^2 f_3(v)$.

The one-dimensional distribution function $f_1(v_z)$ is obtained from the two-temperature distribution by an integration over velocities v_r in the plane perpendicular to z. The two-temperature distribution is first expressed in cylindrical velocity coordinates (v_r, v_z),

$$F_3(v_r,v_z) = n\left(\frac{m}{2\pi T_1}\right)^{3/2}\exp\left(\frac{-m(v_r^2+v_z^2)}{2T_1}\right), \quad \frac{1}{2}m(v_r^2+v_z^2) < \epsilon_t$$
$$= n\left(\frac{m}{2\pi T_1}\right)^{3/2}\exp\left(\frac{-m(v_r^2+v_z^2)}{2T_2}+\frac{\epsilon_t}{T_2}-\frac{\epsilon_t}{T_1}\right), \quad \frac{1}{2}m(v_r^2+v_z^2) \geq \epsilon_t. \quad (27)$$

This distribution is integrated with $2\pi v_r dv_r$ to obtain the one-dimensional distribution $f_1(v_z)$. The projected distribution does not contain a discontinuity in the slope at ϵ_t because the v_z value at which the slope changes depends upon the value of v_r.

The current to the disk probe is calculated at 0.1 V intervals from $f_1(v_z)$ using Eq. (3). The result (not shown) is identical to that obtained from the corresponding speed distribution $\rho(v)$ and Eq. (10). The distribution function $f_1(v_z)$ is recovered from the calculated probe current using Eq. (6) and is plotted in Fig. 1(a) with the original distribution. The speed distribution $\rho(v)$ is recovered using Eq. (12) and compared with the original distribution in Fig. 1(b). The temperatures associated with the two-temperature distribution are most easily found from the slopes of a semilogarithmic plot of $f_3(v)=\rho(v)/4\pi v^2$, which is shown in Fig. 1(c). In all cases, the recovered distribution function (points) is nearly identical to the starting distribution (solid lines).

A quantitative measure of the accuracy of the recovered distributions is the accuracy of the densities obtained by integration. The plasma density obtained from the derived speed distribution using Eq. (13) is 0.94×10^{14} m^{-3}. The plasma density obtained using the first derivative of the current is 0.999×10^{14} m^{-3} for the cubic-spline integration in

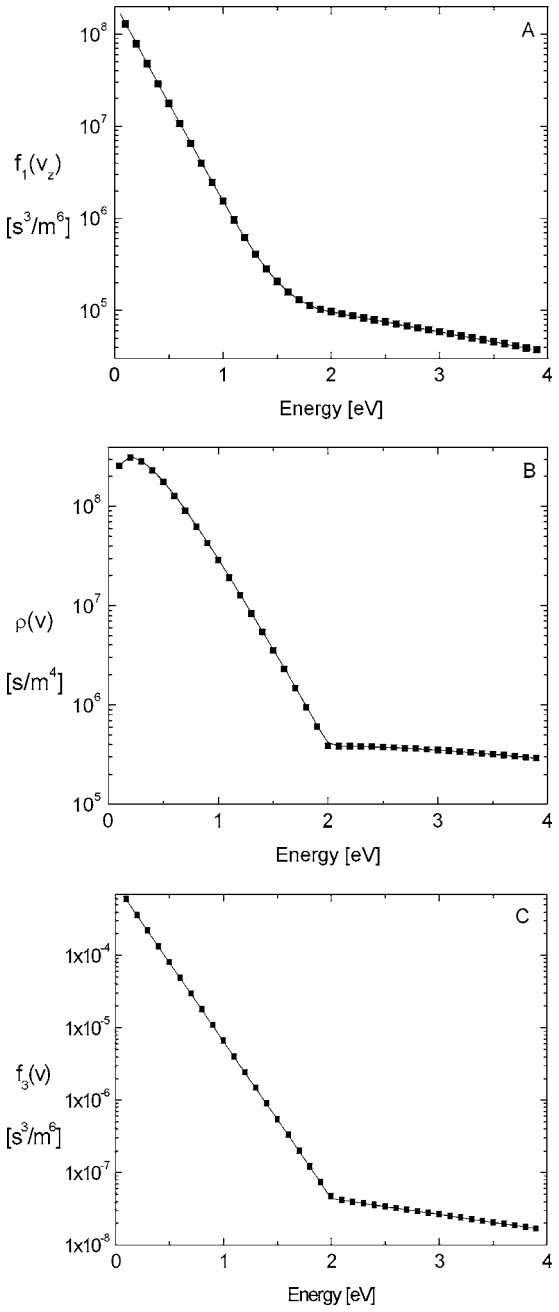

FIG. 1. Distribution functions recovered from simulated disk probe data. (a) Original $f_1(v_z)$ (solid line) and the $f_1(v_z)$ reconstructed from the probe data (squares). (b) Original $\rho(v)$ (solid line) and the reconstructed $\rho(v)$ (squares). (c) The distribution $f_3(v) = \rho(v)/4\pi v^2$.

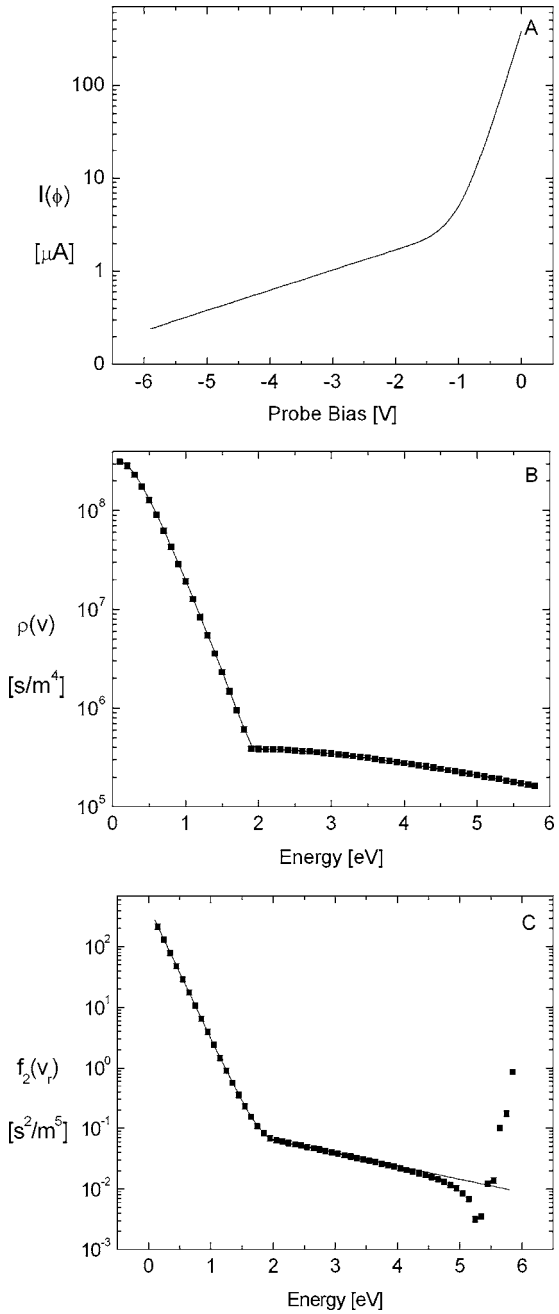

FIG. 2. (a) Current to the cylindrical probe calculated from the model distribution function. The area of the probe is the same as is used in the experiment. (b) The speed distribution $\rho(v)$ (solid line) and the distribution recovered with Eq. (25) (squares). (c) The projected distribution $f_2(v_r)$ (solid line) and the reconstructed distribution from Eq. (20) (squares).

Eq. (7) and 0.76×10^{14} m^{-3} for the Simpson's rule integration of the same integrand.

For the cylindrical probe, the distribution of velocities in the plane perpendicular to the probe axis is obtained by integrating $F_3(v_r, v_z)$ with dv_z. The calculated current to the cylindrical probe, from Eq. (16), is shown in Fig. 2(a). The speed distribution $\rho(v)$ recovered from the current using Eq. (25) is shown in Fig. 2(b). The projected distribution $f_2(v_r)$ from Eq. (20) is shown in Fig. 2(c). The result for the projected distribution is inaccurate at the highest electron energies because the sum cannot be started at an infinitely negative probe voltage. The initial points oscillate about the correct value and converge to within about 1% of the correct value after about 20 data points. Except for these points, the two recovered distributions (points) are nearly identical to the starting distributions (solid lines).

The plasma density obtained from the integration of the projected distribution by Eq. (22) is 0.985×10^{14} m^{-3}. The first 10 points at the highest electron energies are omitted in

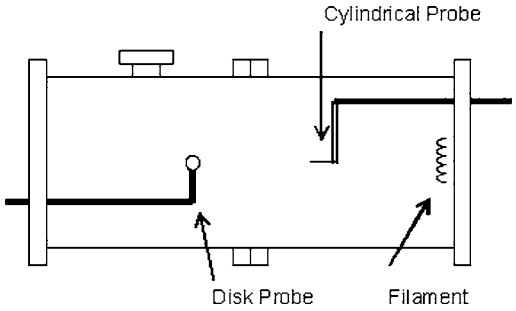

FIG. 3. The experimental apparatus (not to scale). The magnets for the multidipolar field are not shown.

the sum and this omission has less than 1% effect on the density. The plasma density obtained from the recovered speed distribution using Eq. (13) is 0.94×10^{14} m^{-3}. For both types of probes, there are thus two accurate numerical methods for recovering the electron density from the probe data.

IV. ANALYSIS OF EXPERIMENTAL DATA

The methods are applied to probe data from a plasma generated in a multidipolar plasma device [8], Fig. 3, with a diameter of 31 cm and a length of 69 cm. This device has a liner of stainless steel with magnetic line cusps [9,10] of nickel-plated rare-earth magnets (12.5 mm diam$\times$3 mm). The magnets are mounted to iron strips riveted to the liner. The strips have a spacing of 75 mm, the magnet center-to-center spacing is 18 mm, and the field at the magnet surfaces is 0.3 T. The stainless steel liner provides a uniform wall potential that results in a sharp boundary (in energy) between the electrons that are confined by the plasma potential and the secondary electrons from the wall [11,12]. The plasma is created in 0.4 mTorr argon by 16 mA emission from a filament at one end that is biased to −60 V. A two-temperature distribution is clearly seen at low emission currents ($<$100 mA), which results in the largest difference in temperature between the confined electrons ($<$1 eV) and unconfined wall secondaries ($\sim$3 eV). The vacuum is created by a turbomolecular pump and the base pressure is $<10^{-6}$ Torr.

A cylindrical probe and a disk probe are used for measurements. The cylindrical probe has a radius of 95 μm and a length of 30 mm. A relatively long probe is used to have a signal-to-noise ratio that is comparable to that for the disk probe. The cylindrical probe radius is less than the Debye length (0.4 mm) which is required for accuracy of the OML theory. The disk probe is of thin foil with a radius of 3.4 mm that is much greater than the Debye length to minimize edge effects. Both probes are of stainless steel and are discharge-cleaned before data are taken. The probe voltage is swept in 0.1 V increments from −40 to +6 V. The current at each point in the sweep is digitized 25 times and the average is recorded. If the distribution function is to be determined, 64 sweeps are made in a 40 min period and averaged in order to further reduce the noise.

The plasma potential is found as the voltage for which the slope of the data is greatest [7]. The plasma potential is found with better resolution than the voltage spacing $\Delta\Phi$ by fitting a polynomial locally to the data and solving for the zero point of the second derivative. A new grid is constructed having the plasma potential at the origin and the probe current on the new grid is found from the data by linear interpolation. The new grid allows integrals or summations to be ended more precisely at the plasma potential while maintaining a uniform grid spacing.

A. Planar disk probe data

An average of 64 disk probe data sets is plotted in Fig. 4(a). The plasma potential is determined and linear interpolation is used to shift the data to a new grid that has the plasma potential at the origin. A model is fit to the ion current [13] for voltages from −40 to −20 and the modeled ion current is subtracted to give the current from electrons alone shown in Fig. 4(b). The electron data are first analyzed by assuming that the electron current arises from two Maxwellian distributions [14]. The temperature of the cold electron component is determined from the slope of a semilogarithmic plot (avoiding the tail of the distribution) and the density is determined from the saturation current at the plasma potential. This is further refined by using a least-squares method to find the two densities and two temperatures that best fit the data. A distribution function is constructed by summing the "hot" and "cold" Maxwellians. The electron density is then the sum of the densities of the two distributions. The contribution of the hot distribution to the density is typically about 3% of the total. This two-temperature Maxwellian is used as the reference distribution. The low-temperature part of the distribution spans 3.0 eV, thus the plasma potential is presumed to be 3.0 V.

The projected distribution function $f_1(v_z)$ obtained from Eq. (6) is plotted in Fig. 4(c). The points lie near to the two-temperature reference Maxwellian that has temperatures of 0.77 and 2.9 eV. The recovered distribution is relatively free of noise. The speed distribution $\rho(v)$ from the Druyvesteyn method, Eq. (11), is plotted in Fig. 4(d). This distribution is more noisy and detail is lost for energies $\geq$3 eV. The heavy solid line in Fig. 4(d) is obtained using the Savitzky-Golay method [15]. This method is applied by fitting a parabola to groups of five consecutive data points and finding the second derivative in Eq. (11) from the fitted polynomial. The heavy solid line lies near the two-Maxwellian fit. The densities determined from Eq. (7) and (13), and from the two-Maxwellian fit are compared in Table I. The densities differ by less than 10% and thus are consistent.

B. Cylindrical probe data

An average of 64 sweeps of the cylindrical probe, in the same plasma as for Fig. 4, is shown in Fig. 5(a). The averaged data with the ion current removed are shown in Fig. 5(b). The cylinder probe data and the disk probe data differ qualitatively only in the saturation region where the disk probe saturates more quickly. The low-temperature part of the distribution spans 3.1 eV, thus the plasma potential appears to be 3.1 V, which is near to the value of 3.0 V obtained from the disk probe data. The analysis of the cylindrical probe data by the new method, Eq. (20), yields a

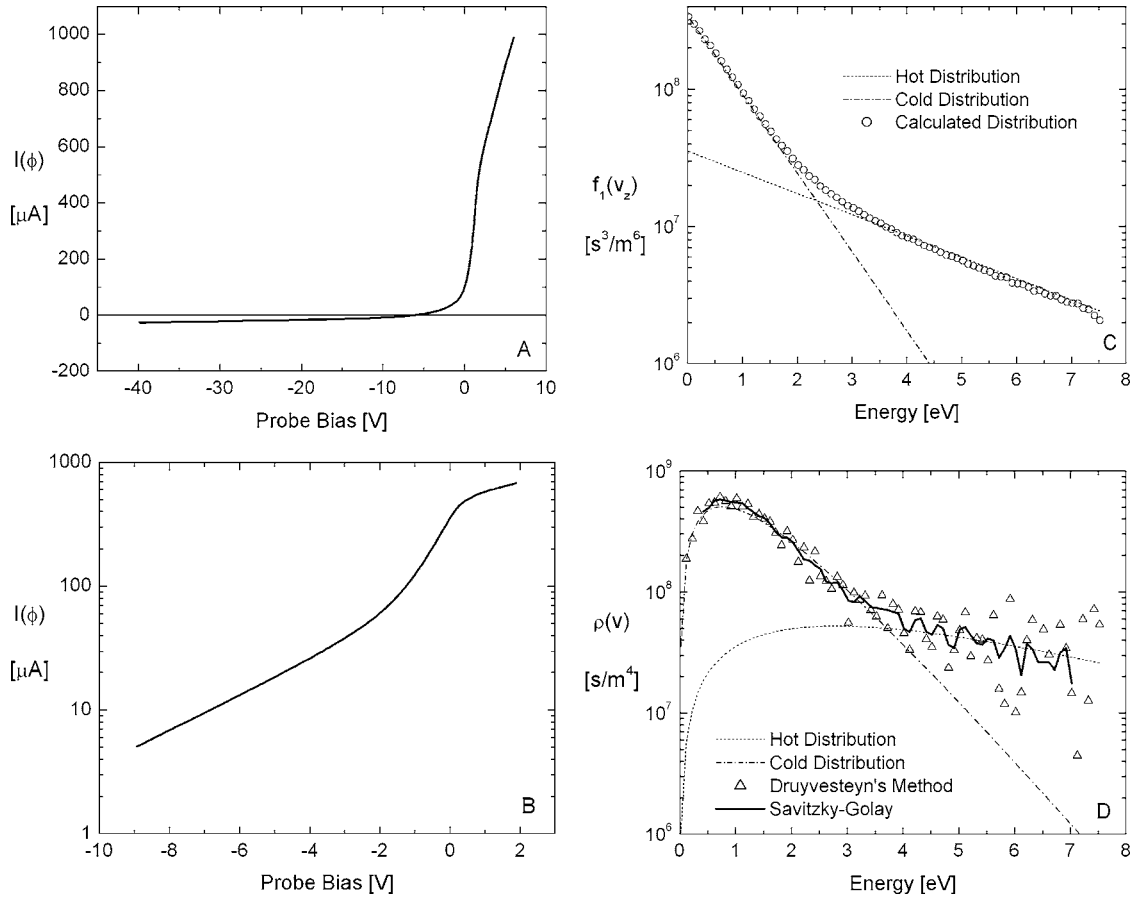

FIG. 4. Analysis of averaged data for the disk probe. (a) The probe current as a function of voltage obtained by averaging 64 data sets. (b) The probe current with the ion contribution removed, showing the two-temperature distribution. (c) The distribution function $f_1(v_z)$ from Eq. (6) (circles). (d) The speed distribution $\rho(v)$ from Eq. (11) (triangles). The distribution obtained using the Savitzky-Golay method to find the second derivative is the solid line. In (c) and (d), the best-fit "hot" and "cold" Maxwellian distributions are shown as dashed and dot-dashed lines, respectively.

projected distribution $f_2(v_r)$ that agrees well with the two-temperature Maxwellian fit, Fig. 5(c). The noise becomes significant for energies greater than about 5 eV. Analysis of the probe data by Druyvesteyn's method, Eq. (25), yields the speed distribution shown in Fig. 5(d). The noise becomes significant between 3 and 4 eV and is only slightly improved by the Savitsky-Golay method of finding the second derivative. The densities obtained from the two-Maxwellian fit and from the two distribution functions are compared in Table I.

TABLE I. Comparison of electron densities determined by the different methods.

Disk probe	
Two-Maxwellian fit	1.93×10^{14} m^{-3}
from $f_1(v_z)$, Eq. (7)	1.88×10^{14} m^{-3}
from $\rho(v)$, Eq. (13)	1.83×10^{14} m^{-3}
Cylinder probe	
Two-Maxwellian fit	2.27×10^{14} m^{-3}
from $f_2(v_r)$, Eq. (22)	2.08×10^{14} m^{-3}
from $\rho(v)$, Eq. (13)	2.04×10^{14} m^{-3}

The densities from the cylindrical probe data are systematically higher than those from the disk probe. The areas of the probes were measured to within a few percent, thus the difference cannot be accounted for by error in the probe areas.

V. DISCUSSION AND CONCLUSION

Methods for finding the electron distribution function and the electron density have been compared for both disk and cylindrical probes. In our double-plasma device with multidipolar fields, the probe current contains two electron contributions at energies below 10 eV. The first contribution, with energies 0–3 eV, is from the confined electrons with energies below the plasma potential. The second contribution is from secondary electron emitted by the walls. The second distribution begins to contribute at the energy corresponding to the plasma potential and the slope of the speed distribution should change discontinuously at this energy. The reference method for analyzing the probe data is to assume that the data are from the sum of two Maxwellian distributions and to find the two temperatures and densities that best fit the data.

Analysis of the disk probe data, Fig. 4, for the projected distribution $f_1(v_z)$ finds a distribution that agrees well with

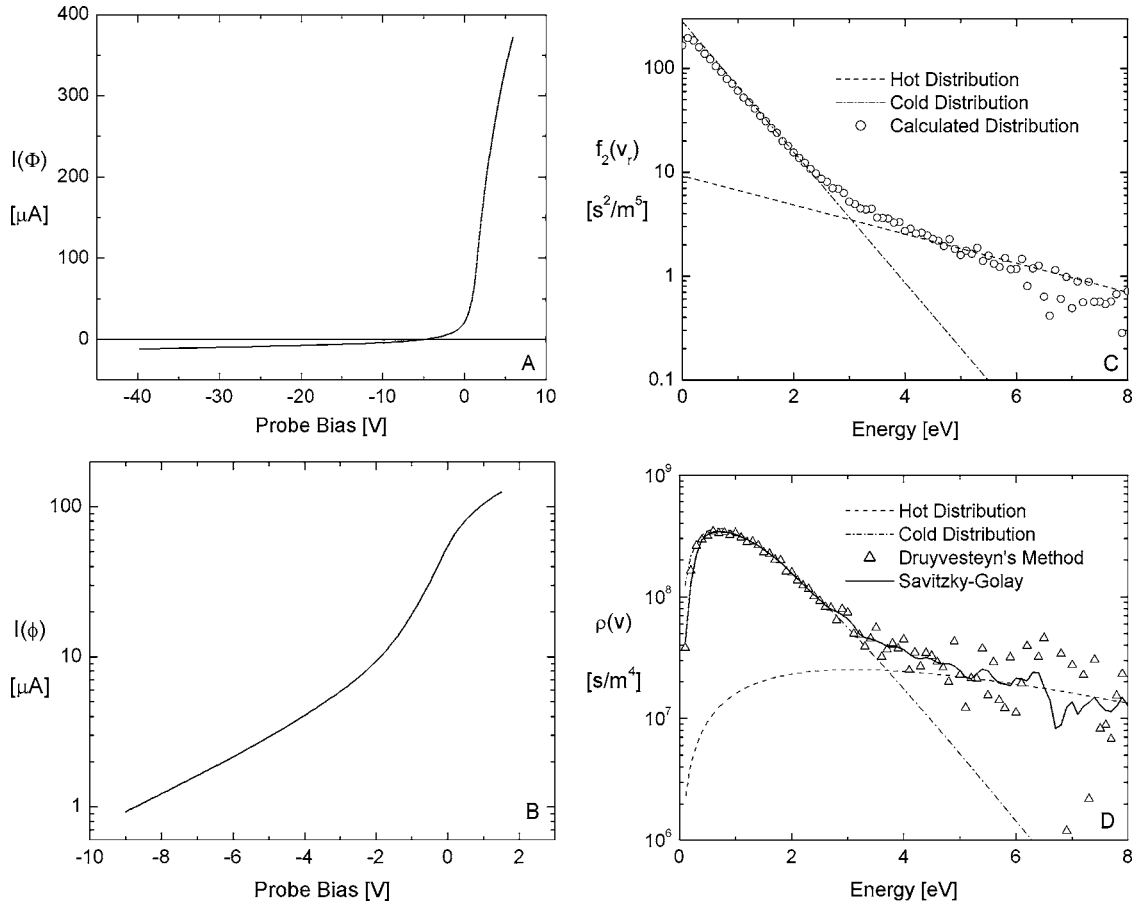

FIG. 5. Analysis of averaged data for the cylindrical probe. (a) The probe current as a function of voltage. (b) The probe current with the ion contribution removed, showing the two-temperature distribution. (c) The distribution function $f_2(v_r)$ from Eq. (20) (circles). (d) The speed distribution $\rho(v)$ from Eq. (11) (triangles). This distribution obtained using the Savitzky-Golay method to find the second derivative is the solid line. In (c) and (d), the best-fit "hot" and "cold" Maxwellian distributions are shown as dashed and dot-dashed lines, respectively.

the corresponding distribution from the two-temperature analysis. Druyvesteyn's analysis for the speed distribution agrees with the two-Maxwellian analysis but is noisy because the second derivative is used. Inspection shows that the energy at which the two distributions join cannot be accurately determined from Druyvesteyn's analysis. This determination is possible using the projected distribution and is most easily done from the two-Maxwellian fit. The two-Maxwellian fit shows the value of a model having only a few parameters (two densities, two temperatures) that can be fit using the data. The Druyvesteyn analysis for the cylinder probe, Fig. 5(d), has a level of noise that is not significantly different from that for the disk probe. The new method for the cylindrical probe, Fig. 5(c), is less noisy than Druyvesteyn's method, but more noisy that the disk probe analysis using the first derivative.

The experimenter is likely to choose the analysis that is most directly related to the physics issues being addressed. For discharges in cylindrical tubes that are long in comparison with their radius, the distributions $f_1(v_z)$ from disk probes and $f_2(v_r)$ from cylindrical probes may be quite different. The data from a single-sided disk probe oriented perpendicular to the cylindrical axis and analyzed using Eq. (5) would correctly recover $f_1(v_z)$ for the direction incident upon the probe. In a dc discharge, this analysis made both parallel and antiparallel to the electric field should show asymmetry caused by the electric field. Data from a cylindrical probe oriented parallel to the tube axis would allow recovery of $f_2(v_r)$ and this distribution should show any truncation of the tail of the distribution from losses of high-energy electrons not contained by the plasma potential. In the derivation of $f_2(v_r)$ from the cylindrical probe data, the velocity v_z is integrated at the outset, thus any drift along the z axis does not change the analysis for $f_2(v_r)$. If the drift is in the plane perpendicular to the z axis, the cylindrical symmetry is destroyed and there is no simple approach for determining $f_2(v_r)$. The analysis for the speed distribution $\rho(v)$ is made assuming an isotropic distribution, thus the formulas that recover $\rho(v)$ from planar or cylindrical probes would not be accurate for an anisotropic distribution. The analyses for the projected distributions $f_2(v_r)$ and $f_1(v_z)$, on the other hand, will not show features at particular energies because these would be "averaged out" by the projection.

[1] M. J. Druyvesteyn, Z. Phys. **64**, 781 (1930).
[2] V. A. Godyak, R. B. Piejak, and B. M. Alexandrovich, Plasma Sources Sci. Technol. **1**, 36 (1992).
[3] V. I. Demidov, S. V. Ratynskaia, and K. Rypdal, Rev. Sci. Instrum. **73**, 3409 (2002).
[4] M. J. Druyvesteyn and N. Warmoltz, Philos. Mag. **17**, 1 (1934).
[5] L. Boltzmann, *Lectures on Gas Theory* (University of California Press, Berkeley, 1964), p. 225.
[6] H. M. Mott-Smith and I. Langmuir, Phys. Rev. **28**, 727 (1926).
[7] See, for example, N. Hershkowitz, *How Langmuir Probes Work*, in Plasma Diagnostics, edited by O. Auciello and D. Flamm (Academic, San Diego, 1989), p. 113.
[8] R. J. Taylor, K. R. Mackenzie, and H. Ikezi, Rev. Sci. Instrum. **43**, 1675 (1972).
[9] K. N. Leung, T. K. Samec, and A. Lamm, Phys. Lett. **51A**, 490 (1975).
[10] L. N. Leung, N. Heshkowitz, and K. R. MacKenzie, Phys. Fluids **19**, 1045 (1976).
[11] S. Robertson, Z. Sternovsky, and B. Walch, Phys. Plasmas **11**, 1753 (2004).
[12] S. Robertson and Z. Sternovsky, Phys. Rev. E **72**, 016402 (2005).
[13] Z. Sternovsky, S. Robertson, and M. Lampe, J. Appl. Phys. **94**, 1374 (2003).
[14] Z. Sternovsky and S. Robertson, Phys. Plasmas **11**, 3610 (2004).
[15] A. Savitzky and M. J. E. Golay, Anal. Chem. **36**, 1627 (1964).